

# Impact of Assimilating Radiances with the WRFDA ETKF/3DVAR Hybrid System on Prediction of Two Typhoons in 2012

XU Dongmei<sup>1,2\*</sup> (许冬梅), HUANG Xiang-Yu<sup>2</sup> (黄向宇), WANG Hongli<sup>2,3</sup> (王洪利), Arthur P. MIZZI<sup>2</sup>,  
and MIN Jinzhong<sup>1</sup> (闵锦忠)

<sup>1</sup> Collaborative Innovation Center on Forecast and Evaluation of Meteorological Disasters, Nanjing University  
of Information Science & Technology, Nanjing 210044, China

<sup>2</sup> National Center for Atmospheric Research, Boulder, CO 80302, USA

<sup>3</sup> Global Systems Division, Earth System Research Laboratory, NOAA, Boulder, CO 80302, USA

(Received April 2, 2014; in final form August 31, 2014)

## ABSTRACT

The impacts of AMSU-A and IASI (Infrared Atmospheric Sounding Interferometer) radiances assimilation on the prediction of typhoons Vicente and Saola (2012) are studied by using the ensemble transform Kalman filter/three-dimensional variational (ETKF/3DVAR) Hybrid system for the Weather Research and Forecasting (WRF) model. The experiment without assimilating radiance data in 3DVAR is compared with two experiments using the 3DVAR and ETKF/3DVAR hybrid systems to assimilate AMSU-A radiance, respectively. The results show that AMSU-A radiance data have slight positive impacts on track forecasts of the 3DVAR system. When the ETKF/3DVAR hybrid system is employed, typhoon track forecast skills are greatly improved. For 36-h forecasts, the hybrid system has a lower root-mean-square error for wind and temperature at most levels, and specific humidity at low levels, compared to 3DVAR. It is also found that, on average, the use of the IASI radiance data along with AMSU-A radiance data in the hybrid system further increases the track, wind, and specific humidity forecast accuracy compared to the experiment without IASI radiance assimilation.

**Key words:** hybrid system, ETKF, ensemble spread, radiance data, typhoon tracks

**Citation:** Xu Dongmei, Huang Xiang-Yu, Wang Hongli, et al., 2015: Impact of assimilating radiances with the WRFDA ETKF/3DVAR hybrid system on prediction of two typhoons in 2012. *J. Meteor. Res.*, **29**(1), 028–040, doi: 10.1007/s13351-014-4053-z.

## 1. Introduction

A background error covariance (BEC) matrix is intrinsically important in determining the level of influence each observation has on the analysis and how this influence is distributed both spatially and among different analysis variables in data assimilation (DA). Compared to the variational DA approaches (Lorenz, 1986; Parrish and Derber, 1992; Barker et al., 2004), which generally use the time-invariant and nearly-homogeneous BEC, ensemble techniques capture the “errors of the day” that usually propagate in time on multiple scales from short term ensemble forecasts

(e.g., Torn and Hakim, 2009; Zhang et al., 2009; Hamill et al., 2011a). One such approach is the ensemble Kalman filter (EnKF), which was first proposed by Evensen (1994) and has been widely tested in numerical weather prediction (NWP) model experiments against real data (e.g., Dowell et al., 2004; Meng and Zhang, 2008; Whitaker et al., 2008; Zhang et al., 2009; Liu et al., 2012).

The hybrid ensemble/variational DA incorporates the ensemble-produced BEC within a variational framework. Studies by Hamill and Snyder (2000), Lorenz (2003), and Wang et al. (2007, 2008) have demonstrated that the hybrid system has some poten-

Supported by the National (Key) Basic Research and Development (973) Program of China (2013CB430102), National Natural Science Foundation of China (41375025), and Innovation Scientific Research Program for College Graduates of Jiangsu Province (CXZZ12-0490).

\*Corresponding author: xdmjolly@gmail.com.

©The Chinese Meteorological Society and Springer-Verlag Berlin Heidelberg 2015

tial to yield the “the best of two worlds” by improving the deterministic forecasts, due to the inclusion of the flow-dependent BEC and the standalone EnKF with a small ensemble size.

Recently, the hybrid system has been used to study tropical cyclones (TCs) in global (Hamill et al., 2011b) and regional (Wang, 2011, hereafter W11; Li et al., 2012; Schwartz et al., 2013) modeling systems assimilating real observations. All of the above studies found that the hybrid system produced more statistically significant TC tracks and intensity forecasts than those from three-dimensional variational (3DVAR) analyses. Among these studies, W11 reported that static BEC, in particular, was poorer than the flow-dependent BEC in observation-sparse regions. Schwartz et al. (2013) found that the hybrid system with the flow-dependent BEC produced comparable track forecasts to those from 3DVAR analyses with multiple outer loops.

Different from the above studies, which focused on comparisons between the hybrid and the variational systems that assimilate mainly conventional observations, this study explores the effect of satellite radiance assimilation in a hybrid framework on typhoon forecasting. Many of the operational NWP centers assimilate radiance data with variational DA methods. Several studies have also explored the impact of assimilating radiance data for typhoon forecasting within EnKF frameworks (Liu et al., 2012; Schwartz et al., 2012).

The impacts of radiance data on weather forecasting are known to be significant, especially for areas over oceans with sparse conventional observations (Liu et al., 2012). However, the impact of the radiance data in the hybrid data assimilation system is not clear. The purpose of this study is to explore the impact of radiance assimilation on analyses and subsequent forecasts using the Weather Research and Forecasting model DA/ensemble transform Kalman filter (WRFDA/ETKF) hybrid system.

In this study, we choose the ETKF (Bishop et al., 2001) to update the ensemble perturbations, since it is relatively computationally inexpensive to solve the Kalman filter equations in ensemble space and they produce skillful ensembles (W11). This work makes use of radiance data including both microwave and

infrared radiance data in the initialization of the TC environment. This work also differs from W11 in improving the inflation and fraction formula in the ETKF algorithm to stabilize the ETKF when estimating the inflation factors with limited ensemble size. Moreover, sensitivities to vertical correlation localization matrices are also assessed.

The remainder of this paper is organized as follows. In Section 2, we provide a brief introduction to the WRFDA ETKF/3DVAR hybrid system and radiance assimilation methodology. An overview of typhoon cases and the experimental settings are given in Section 3. The results are presented in Section 4. Summary and future perspectives are presented in Section 5.

## 2. The ETKF/3DVAR hybrid system and radiance data assimilation

### 2.1 The ETKF/3DVAR hybrid system

The ETKF/3DVAR hybrid system is a component of the WRFDA system (Barker et al., 2012). The hybrid analysis increment  $\delta\mathbf{x}$  is defined as the sum of two terms,

$$\delta\mathbf{x} = \delta\mathbf{x}_{\text{static}} + \delta\mathbf{x}_{\text{flow-dep}}, \quad (1)$$

where the first term  $\delta\mathbf{x}_{\text{static}}$  is the increment associated with the 3DVAR static background covariance and the second term  $\delta\mathbf{x}_{\text{flow-dep}}$  is the increment associated with the flow-dependent covariance given by

$$\delta\mathbf{x}_{\text{flow-dep}} = \sum_{k=1}^N \boldsymbol{\alpha}_k \circ \mathbf{x}'_k, \quad (2)$$

where  $N$  is the ensemble number,  $\boldsymbol{\alpha}_k$  is the extended control variable as defined by Lorenc (2003), and  $\mathbf{x}'_k$  is the  $k$ th ensemble perturbation state vector. The symbol “ $\circ$ ” denotes the Schur product (element by element product) of the vectors  $\boldsymbol{\alpha}_k$  and  $\mathbf{x}'_k$ . The corresponding cost function with respect to  $\delta\mathbf{x}$  and  $\boldsymbol{\alpha}_k$  to obtain the increment is

$$\begin{aligned} J(\delta\mathbf{x}, \mathbf{a}) = & \frac{1}{2}\beta_1(\delta\mathbf{x}_{\text{static}})^T B^{-1}(\delta\mathbf{x}_{\text{static}}) \\ & + \frac{1}{2}\beta_2(\mathbf{a})^T \mathbf{A}^{-1}(\mathbf{a}) + \frac{1}{2}(\mathbf{H}\delta\mathbf{x} - \mathbf{d})^T \\ & \cdot \mathbf{R}^{-1}(\mathbf{H}\delta\mathbf{x} - \mathbf{d}), \end{aligned} \quad (3)$$

where  $\delta\mathbf{x}$  is given by Eqs. (1) and (2),  $\mathbf{a}$  is a vector formed by concatenating  $N$  vectors  $\boldsymbol{\alpha}_k$ , and  $\mathbf{A}$  is a block diagonal matrix that controls the spatial correlation of  $\mathbf{a}$ , effectively performing localization of the ensemble BEC.  $\mathbf{H}$  and  $\mathbf{H}$  are the nonlinear and linearized observation operators, and  $\mathbf{d} = \mathbf{y} - \mathbf{H}\delta\mathbf{x}_b$  is the innovation vector, where  $\mathbf{x}_b$  denotes the background and  $\mathbf{y}$  is the observations. In the WRFDA hybrid system, both the horizontal and vertical localizations in  $\mathbf{A}$  are applied. We found that the results were similar when we set the horizontal localization radius to 500, 750, and 1000 km for the experiments in this study. The results in the following sections are based on 750-km horizontal localization radius. The vertical localization was implemented through transforming the extended control variable with empirical orthogonal functions (EOFs; Li et al., 2012; Wang et al., 2014). The default vertical correlation  $c$  between two levels ( $l_1$  and  $l_2$ ) in released WRFDA is defined as

$$c(l_1, l_2) = \exp\left(-\frac{(l_1 - l_2)^2}{(10\frac{l_1}{M})^2}\right), \quad (4)$$

where  $M$  is the total model level number. The localization radius  $\frac{10l_1}{M}$  is proportional to the model level index, indicating that the localization radii for the lower levels were much smaller than those of the higher levels. For radiance observations, a more advanced correlation method is

$$c(l_1, l_2) = \exp\left(-\frac{(z(l_1) - z(l_2))^2}{r^2}\right), \quad (5)$$

in which a distance  $r$  is directly chosen as the localization radius to fully spread the observation information over the whole model space, even for the low levels, where  $z(l)$  is the height of the model level  $l$ . For radiance assimilation, we conducted sensitivity experiments on vertical localization using Eqs. (4) and (5) with 4- and 8-km localization radii, respectively. The results were not sensitive to the vertical localization schemes (figure omitted). Thus, we determined an 8-km radius for the hybrid model to conduct further comparisons with 3DVAR in the following sections.

The weights of the static covariance and flow-dependent covariance were determined by factors  $\beta_1$

and  $\beta_2$ , with the constraint  $\frac{1}{\beta_1} + \frac{1}{\beta_2} = 1$ . For the experiments in this study, we set  $\frac{1}{\beta_2} = 0.5$ . We weighted the BEC 50% toward the ensemble contribution, although we achieved similar results using 75% and 25%.

In this study, ETKF was used to update the ensemble, estimating forecast error from the covariance matrix of the ensemble forecast perturbations (Bishop et al., 2001). ETKF was described by Wang et al. (2007) as

$$\mathbf{X}^a = \mathbf{X}^b \mathbf{T} \mathbf{\Pi}, \quad (6)$$

where the ETKF transforms the matrix of forecast perturbations  $\mathbf{X}^b$  into a matrix of analysis perturbations  $\mathbf{X}^a$ , whose columns contain  $N$  analysis perturbations  $\mathbf{x}_k^e$  by a transformation matrix  $\mathbf{T}$  with the inflation factor  $\mathbf{\Pi}$ .  $\mathbf{T}$  is chosen to ensure the output ensemble error covariance to precisely equal the true analysis error covariance. The solution of  $\mathbf{T}$  is given by

$$\mathbf{T} = \mathbf{C}(\rho_c \mathbf{\Gamma} + \mathbf{I})^{-1/2} \mathbf{C}^T, \quad (7)$$

where  $\mathbf{C}$  contains the eigenvectors and  $\mathbf{\Gamma}$  the eigenvalues of the  $N \times N$  matrix  $(\mathbf{X}^b)^T \mathbf{H}^T \mathbf{R}^{-1} \mathbf{H} \mathbf{X}^b$ ,  $\mathbf{I}$  is the identity matrix, and  $\rho_c$  is the fraction factor accounting for the projection of the forecast error in ensemble space. For an ensemble size  $N$  of 100 or less, the computational cost of Eq. (7) is relatively low. An enhanced inflation and eigenvector dependent fraction factor scheme (Xu et al., 2013b) was employed to increase the ensemble covariance to ameliorate the underestimation of the analysis-error variance. This scheme is given by

$$\mathbf{T} = \mathbf{C}(\mathbf{p}\mathbf{\Gamma} + \mathbf{I})^{-1/2} \mathbf{C}^T, \quad (8)$$

where the component of the vector  $\mathbf{p} = (\rho(1), \rho(2), \dots, \rho(N))$  is the fraction factor for each eigenvector of the ensemble covariance matrix. Equation (8) is a refined form of Eq. (7). The fraction factors correct the inflation in proportion to the forecast error variance projected onto a particular  $k$ th eigenvector. The adaptive fraction algorithm here aims to ameliorate the problem by distinguishing between

large and small background forecast errors, explained by the different ensemble eigenvectors, instead of using a constant fraction factor to rescale all the eigenvalues. In this study, observations used in ETKF when calculating the transformation matrix were the same as those in the hybrid system, filtered by strict quality control, and only radiosonde measurements were used in estimating the inflation factor.

The procedure for the cycling ETKF/3DVAR hybrid system includes six stages as follows.

(1) Generating the initial ensemble (20 members in this study) by adding the NCEP Global Forecast System (GFS) analysis and correlated random perturbations following Torn et al. (2006) and Wang et al. (2008), before re-centering the ensemble with the GFS analysis; (2) obtaining short-term ensemble forecasts from the initial ensemble in step (1); (3) calculating the ensemble mean and perturbations; (4) updating the ensemble mean and perturbations with the 3DVAR and ETKF, respectively; (5) obtaining an analysis ensemble by adding the updated ensemble mean and perturbations; and (6) updating the lateral boundary conditions and lower boundaries before conducting short-term ensemble forecasts to the next assimilation time or run a deterministic forecast to diagnose outputs from the analysis ensemble mean, and repeat from step (3).

## 2.2 Radiance assimilation procedures

The community radiative transfer model (Han et al., 2006; Liu and Weng, 2006) was used as the observation operator  $\mathbf{H}$  in WRFDA for computing radiances from the model profiles of temperature and moisture (Barker et al., 2012). A radiance observation was rejected if the bias-corrected innovation (observation minus prior) exceeded either 15 K or  $3\sigma_0$ , where  $\sigma_0$  is the specified observation error standard deviation for brightness temperature. Radiance data over mixed surfaces (e.g., over coastal areas) and observations with large scan angles (the first two pixels for AMSU-A radiances and the first four pixels for IASI radiances on the edge) were rejected. In these experiments, radiance data were used with a 90-km thinning mesh. Data within  $\pm 2$  h of the analysis times were

used and assumed to be valid at the analysis times. For the IASI infrared radiance data, the algorithm developed by McNally and Watts (2003) was used for cloud detection (Xu et al., 2013a).

The systematic errors for radiance observations were corrected by modifying the observation operator  $\mathbf{H}$  as follows:

$$\mathbf{H}^{\text{BIAS}}(\mathbf{x}, \gamma) = \mathbf{H}(\mathbf{x}) + \gamma_0 + \sum_{i=0}^{I_p} \gamma_i p_i(\mathbf{x}), \quad (9)$$

where  $\gamma_0$  is the constant component of total bias,  $I_p$  the number of the potentially state-dependent predictors, and  $p_i$  the predictors (the scan position, the square and cube of the scan position, the 1000–300- and 200–50-hPa layer thicknesses, surface skin temperature, and total column water vapor) and their coefficients  $\gamma_i$  (Liu et al., 2012). The coefficients were updated by a variational minimization process by including them as control variables (Derber and Wu, 1998; Auligné et al., 2007; Dee and Uppala, 2009).

## 3. Overview of cases and experimental design

To evaluate the impact of radiance data assimilation in the WRFDA ETKF/3DVAR hybrid system with flow-dependent background error, analysis/forecast experiments with radiance assimilation are performed over the period from 18 July to 1 August 2012, during which time typhoons Vicente and Saola formed (Fig. 1).

### 3.1 Vicente and Saola (2012)

Typhoon Vicente was one of the most powerful storms to strike southern China in recent years, causing major damage to life and property. Vicente began as a tropical depression on 18 July 2012, northeast of the Philippines. Vicente steadily moved into the South China Sea, and gradually strengthened throughout 23 July, at which point it changed course towards Guangdong Province. Later on the same day, Vicente made landfall over Taishan, Guangdong.

Typhoon Saola was a tropical cyclone that affected the Philippines and China (including the Taiwan region). On 26 July, a tropical depression developed about 1000 km to the southeast of Manila. On

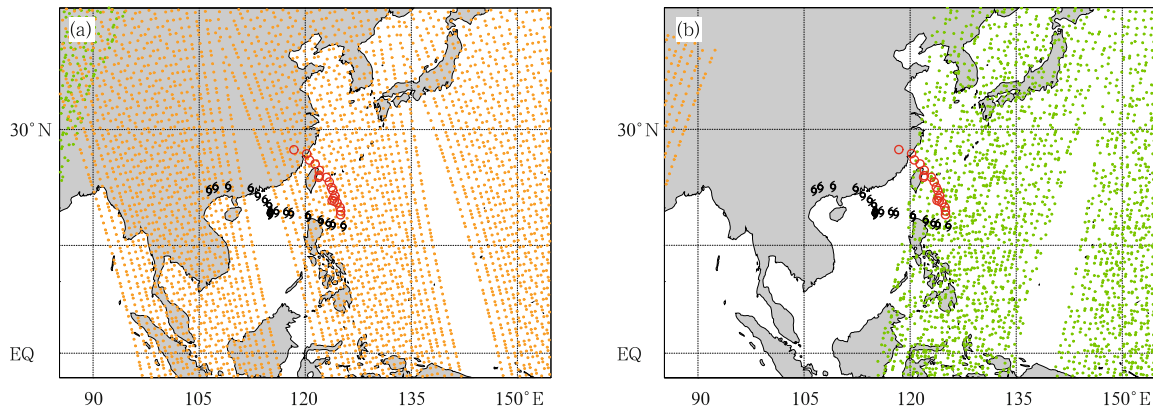


**Fig. 1.** The WRF model domain and the 6-h tracks of Typhoon Vicente (black typhoon symbols) from 0000 UTC 20 to 0000 UTC 25 July, and Typhoon Saola (red circles) from 1800 UTC 29 July to 0600 UTC 3 August. The snapshot of AMSU-A (orange dots from NOAA-18) and IASI (green dots from MetOp-A) radiance observations available within the assimilation window time of the first analysis time are denoted valid at (a) 0600 UTC 18 and (b) 0000 UTC 19 July 2012, respectively.

28 July, it was upgraded to a tropical storm, and to a category-1 typhoon on 30 July. It was soon downgraded to a tropical storm late on 30 July. On 31 July, Saola developed again into a category-1 typhoon, and then to a category-2 typhoon early the next day. Typhoon Saola made landfall over Taiwan at 1920 UTC 1 August. On 2 August, Saola was downgraded to a tropical storm and made landfall again over Fujian at 2250 UTC.

### 3.2 Experimental design

#### 3.2.1 WRF model

The WRF model (version 3.5; Skamarock et al., 2008) is employed in all forecast experiments. The following physical schemes are used: the WRF single-moment 5-class microphysics scheme (Hong et al., 2004); the Goddard shortwave (Chou and Suarez, 1994) and rapid radiative transfer model (RRTM) longwave (Mlawer et al., 1997) radiation schemes, including the refined upper boundary condition for RRTM (Cavallo et al., 2011), necessary when cycling model tops above 50 hPa; the Yonsei University boundary layer scheme (Hong et al., 2006); the Noah land surface model (Chen and Dudhia, 2001); and the Kain-Fritsch cumulus parameterization (Kain and Fritsch, 1990). The model domain for the experiments, as shown in Fig. 1, has an 18-km grid spacing on a  $400 \times 300$  horizontal grid cell and 43 vertical lev-

els, with the model top at 10 hPa.

#### 3.2.2 Data assimilation experiments

Microwave and infrared radiance data are two major sources of satellite data, and both are important observation types for data assimilation, especially for areas over oceans with sparse conventional observations. As two representative sources of microwave and infrared radiance data, AMSU-A and IASI (Infrared Atmospheric Sounding Interferometer) radiances are widely studied in 3DVAR or EnKF frameworks (McNally, 2007; Liu et al., 2012; Schwartz et al., 2012; Xu et al., 2013a). In this study, five experiments are carried out to assess the influences of AMSU-A and IASI data on typhoon forecasts (Table 1), using both the 3DVAR and the ETKF/3DVAR hybrid system. The first three experiments, denoted as CTRL, 3DVAR\_AM, and HYBRID\_AM are conducted to evaluate the AMSU-A data impacts. The experiment CTRL assimilates only conventional observations from the NCEP operational global telecommunication system dataset with 3DVAR. The experiment 3DVAR\_AM, similar to CTRL, assimilates AMSU-A radiances from NOAA-18 and MetOp-A besides the conventional observations in CTRL. The experiment HYBRID\_AM assimilates all observations from the experiment 3DVAR\_AM, but with the hybrid system. The distribution of AMSU-A observations available for the first cycle time is shown in Fig. 1.

**Table 1.** Descriptions of experiments

Experiment	Assimilation system	Observations
CTRL	3DVAR	Conventional observations
3DVAR_AM	3DVAR	Conventional observations + AMSU-A radiance (NOAA-18 and MetOp-A)
HYBRID_AM	ETKF/3DVAR hybrid	Same as 3DVAR_AM
3DVAR_AMIA	3DVAR	Conventional observations + AMSU-A radiance (NOAA-18 and MetOp-A) + IASI radiance (MetOp-A)
HYBRID_AMIA	HYBRID	Same as 3DVAR_AMIA

The IASI (Blumstein et al., 2004) is an advanced sensor, providing observational atmospheric temperature and humidity data with unprecedented accuracy and resolution. Xu et al. (2013a) found that including IASI radiance data improved TC forecasts, especially for TC tracks in 3DVAR. Assimilation effects of both AMSU-A and IASI radiances on typhoons in the hybrid framework are explored to discover the extent to which IASI radiances will be complementary or redundant to AMSU-A radiances in the hybrid framework. Two extra experiments 3DVAR\_AMIA and HYBRID\_AMIA are conducted, similar to experiments 3DVAR\_AM and HYBRID\_AM, respectively, but also assimilate IASI radiances from MetOp-A with channels around  $15.0 \mu\text{m}$ .

Forecast-analysis experiments are carried out on a 6-h cycling basis. The data assimilation period is from 0600 UTC 18 July to 0000 UTC 1 August 2012. We compute the BEC statistics provided by the NMC method (Parrish and Derber, 1992) by using the differences in the 24- and 12-h forecasts initiated from GFS analyses at 0000 and 1200 UTC every day from 1 to 30 July 2011. During this period, four typhoons that formed in the western Pacific Ocean struck eastern China. The BEC statistics could have been derived from any one of these four. The background ensemble in the first analysis is provided by the 6-h ensemble forecast initiated from the NCEP GFS  $0.5^\circ \times 0.5^\circ$  analysis at 0000 UTC 18 July. The forecast ensemble is then re-centered about the GFS analysis, shifting the ensemble mean to preserve the perturbations about the mean. For the following cycles, the background is a 6-h WRF forecast from the previous cycle. The lateral boundary conditions for the WRF forecasts are also provided by the operational GFS forecasts at 3-h intervals. In total, there are 56

analyses and forecasts during the period.

## 4. Results

### 4.1 Ensemble performance

The key to ensemble-based DA is the use of an ensemble to estimate the forecast error in a flow dependent manner, so it is important to briefly examine the ensemble performance. The ensemble spread of wind and temperature at the 9th model level is shown in Fig. 2 after 2-day cycles valid at 0000 UTC 20 July, when Typhoon Vicente formed. The ensemble spread reveals patterns that reflect features of the meteorological conditions and observation locations. Great spread is found over western China, where few observations are available to constrain the model. A local spread maximum is evident for wind speed and temperature in the northeast of the Philippines, where the TCs moved, reflecting the uncertainty of TC prediction.

In a well-calibrated system, the ensemble mean root-mean-square error (RMSE) compared to observations (or other reference) equals the “total spread” (Houtekamer et al., 2005). The forecast RMSEs, with a total spread aggregated between 0000 UTC 19 and 0000 UTC 31 July, and the static background error (defined as CV\_5) calculated by the “gen\_be” utility in WRFDA (Wang et al., 2014) using the NMC method are shown in Figs. 3a and 3b. The forecast RMSEs are assessed by comparing the forecast ensemble mean to the GFS analyses. We generate a 200-member ensemble by sampling the background error with Gaussian noise using the random-cv facility in WRFDA. The static background errors in Fig. 3 are estimated based on the ensemble perturbations in the 200 members. The averaged wind and temperature

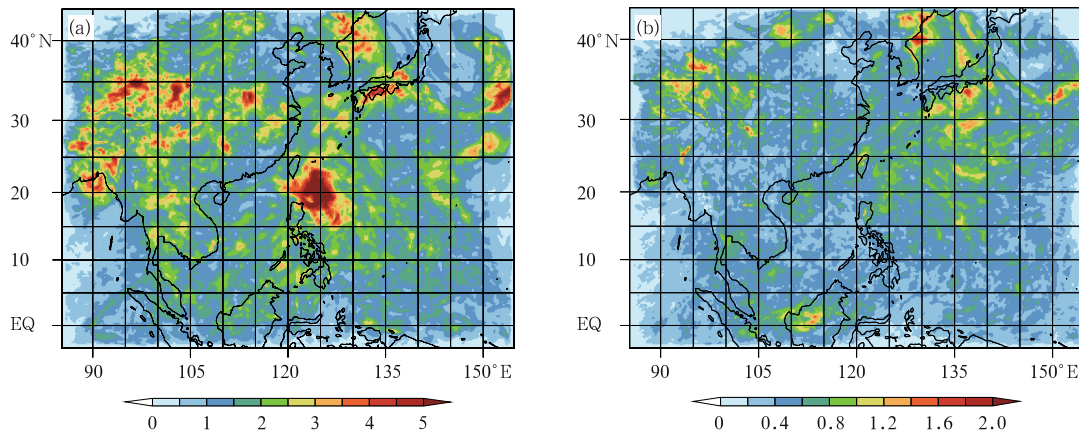


**Fig. 2.** Ensemble spread for (a) wind speed ( $\text{m s}^{-1}$ ) and (b) temperature (K) valid at 0000 UTC 20 July 2012 at the 9th model level.

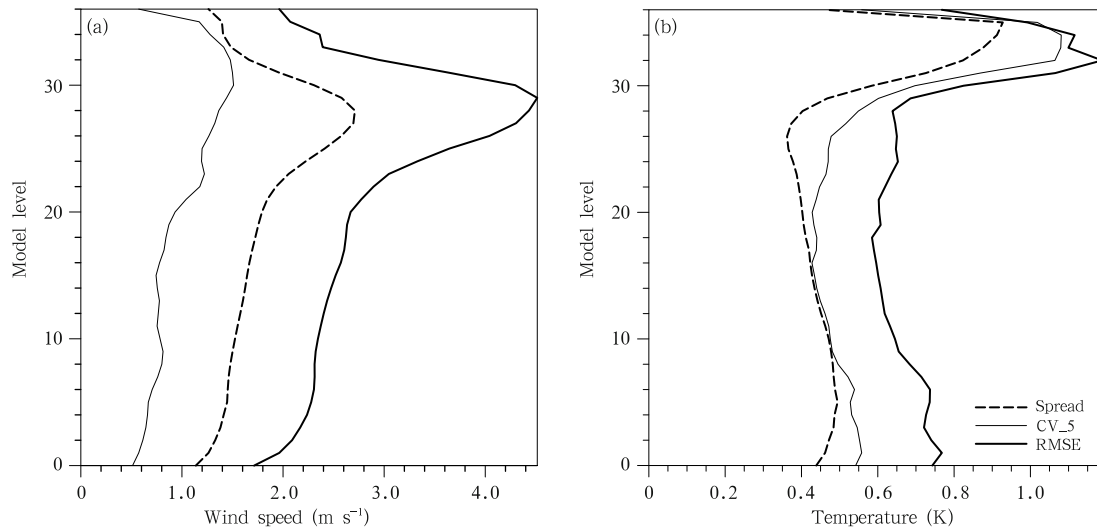


**Fig. 3.** Static background error (CV\_5), averaged forecast RMSEs against GFS analyses, and averaged ensemble spread at 0000 UTC 19 July and 0000 UTC 1 August for (a) wind speed ( $\text{m s}^{-1}$ ) and (b) temperature (K).

forecast RMSEs are less than  $3 \text{ m s}^{-1}$  and  $1 \text{ K}$  for most levels. For winds, the static BEC calculated with the NMC method is largely underestimated, also found by Wang et al. (2014), whereas the ensemble spread is in between the RMSEs and the static BEC. The ensemble lacks sufficient spread in temperature, especially for the low levels. The increment from assimilation is probably small where spread is small, indicating less forecast uncertainty. The final BEC from the hybrid system, as a mix of the flow-dependent and the static BEC, plays an important role in the data assimilation procedure.

## 4.2 AMSU-A radiance impact

### 4.2.1 Analysis and forecast verification against ERA-Interim reanalysis

The mean differences between the 0000 and 1200 UTC model analyses and corresponding ERA-Interim fields (model minus ERA-Interim) over the experimental period are shown in Fig. 4 for temperature and wind speed. The CTRL analyses exhibit significant warm biases (Fig. 4a) relative to the ERA-Interim over most of the domain, especially along the typhoon tracks, with larger bias values compared to

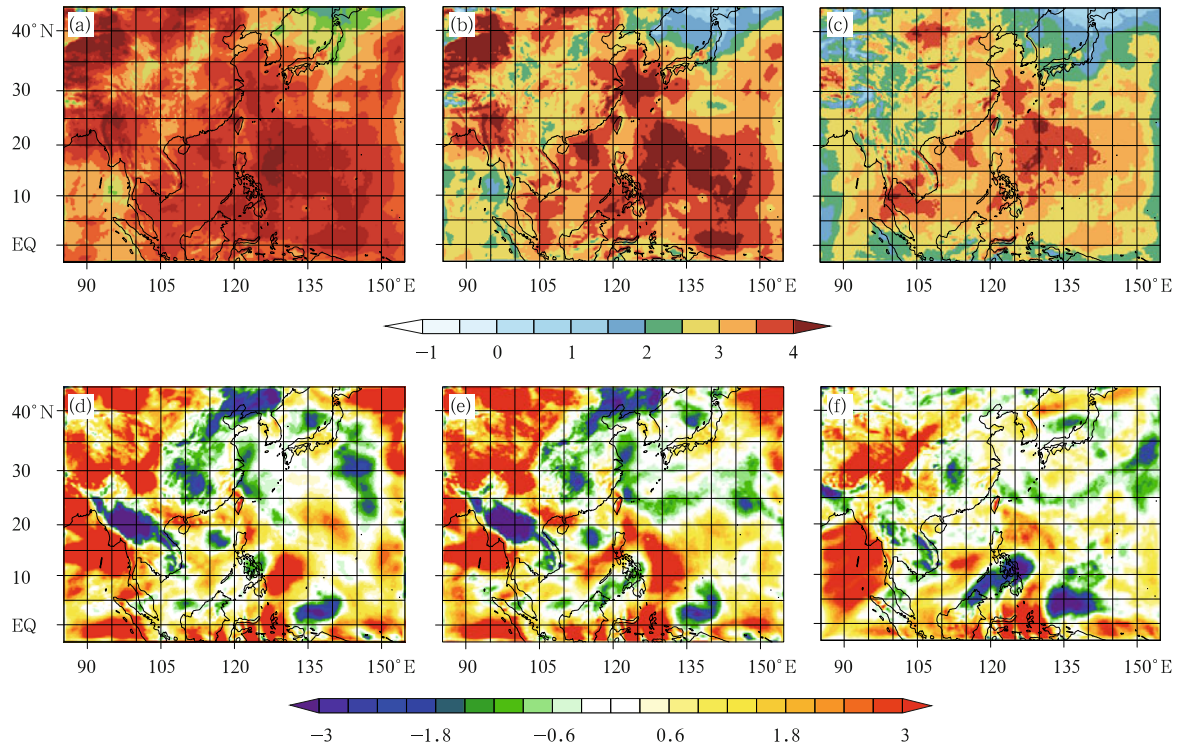


**Fig. 4.** (a, b, c) Averaged temperature (K) and (d, e, f) wind speed ( $\text{m s}^{-1}$ ) bias at the 9th model level for CTRL, 3DVAR\_AM, and HYBRID\_AM against the ERA-Interim over the period 0000 UTC 19 July and 0000 UTC 1 August.

HYBRID\_AM (3.28 versus 2.82), consistent with the results of Liu et al. (2012). Past studies (e.g., Wang et al., 2011; Wang and Huang, 2012) have shown that wind perturbation around TCs plays an important role in TC movements. From Figs. 4c and 4f, it is clear that HYBRID\_AM shows the smallest bias compared to both CTRL and 3DVAR\_AM for both fields, even

over eastern China, where few observations are available, which is achieved through the BEC.

#### 4.2.2 Track forecast verification

Figure 5 shows the 72-h track forecasts initialized at 0000 UTC 21 and 0000 UTC 31 July every 6 hours, respectively. The best track positions from the China Meteorological Administration are also plotted (black

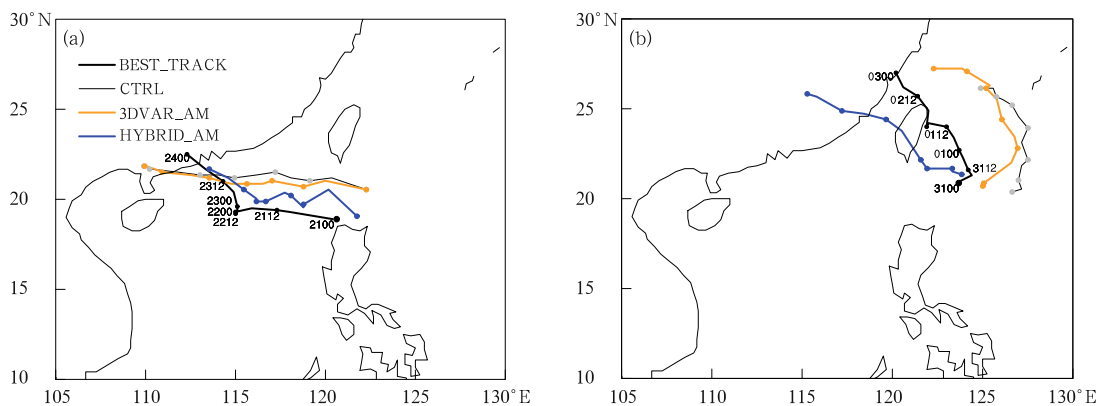


**Fig. 5.** 72-h track forecasts initialized at (a) 0000 UTC 21 and (b) 0000 UTC 31 July 2012 for BEST\_TRACK, CTRL, 3DVAR\_AM, and HYBRID\_AM.

dots). For the forecasts beginning at 0000 UTC 21 July (Fig. 5a), the AMSU-A radiance has a positive impact on the track forecast from both 3DVAR\_AM and HYBRID\_AM, preventing the northward bias. The forecast track from HYBRID\_AM agrees better with the best track than the CTRL and 3DVAR\_AM. The worst track forecast occurs for Saola, with a significant northeastward bias from both 3DVAR experiments. For the forecasts beginning at 0000 UTC 31 July (Fig. 5b), the northeastward biases from the CTRL and 3DVAR\_AM experiments are evident. However, even in these poor forecasts, the hybrid system still upgrades the track forecast, especially for the first 36 hours, though the typhoons moved rather faster after making landfall.

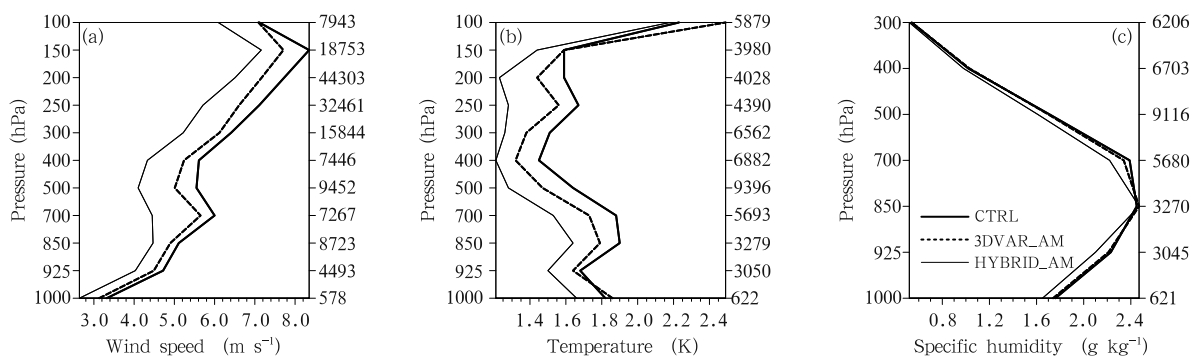
#### 4.2.3 Forecast verification against conventional observations

To assess large-scale performance, 36-h forecasts are verified against a set of conventional observations (radiosondes and GeoAMV) in Fig. 6 from 0000 UTC 20 to 0000 UTC 1 August. Inclusion of AMSU-A radiance data has a positive impact on all the variables in 3DVAR, except for slightly worse temperature forecasts at the very low and high levels. The hybrid experiment agrees better with the observations than the 3DVAR experiment does at almost all levels for wind and temperature and at low levels for specific humidity.

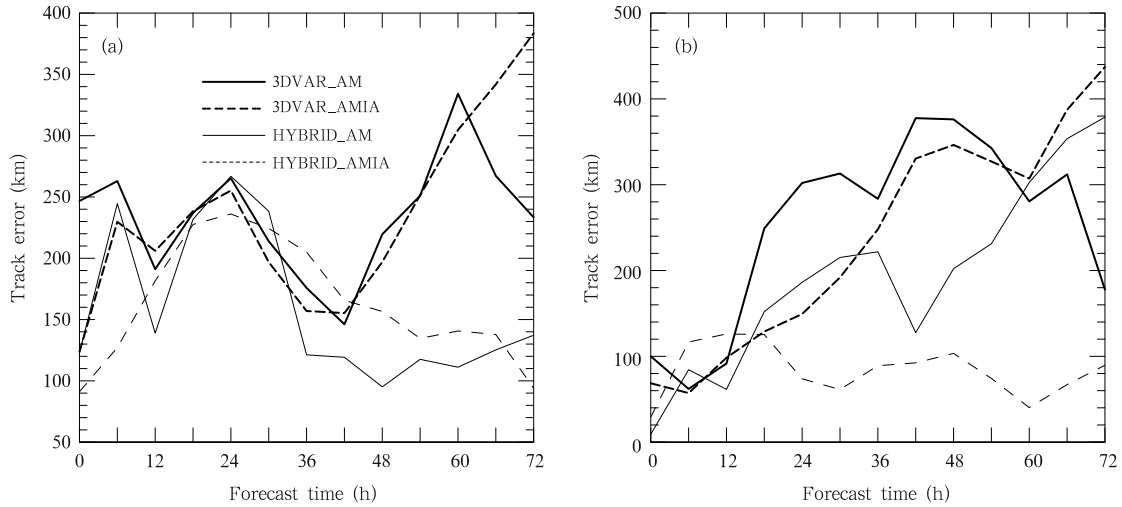
#### 4.3 Added value of IASI radiance data assimilation

Figure 7 shows the absolute track errors of the typhoons for the two 3DVAR experiments (3DVAR\_AM and 3DVAR\_AMIA) and two hybrid experiments (HYBRID\_AM and HYBRID\_AMIA). Consistent with the results from Xu et al. (2013a), the IASI radiance has a steady positive impact on the forecast skill when tracking the 3DVAR framework within approximately the first 54 hours. Generally, track forecasts from the hybrid scheme are better than or at least comparable to those from the 3DVAR system for most forecast hours. HYBRID\_AMIA improves the track forecast for Typhoon Saola more significantly than for Typhoon Vicente in Fig. 7b.

Similar to Fig. 6, Fig. 8 displays the RMSE profiles of the 36-h forecasts verified against a set of conventional observations. Consistent with the results from Xu et al. (2013a), experiment 3DVAR\_AMIA has smaller RMSEs for temperature, wind, and specific humidity at most levels compared to 3DVAR\_AM. Radiance assimilation in the hybrid system dramatically improves forecasts of all variables consistently. The assimilation IASI radiance data can upgrade forecasts of wind and specific humidity at almost all levels. The RMSEs from HYBRID\_AM and HYBRID\_AMIA are comparable for the temperature forecast. One possible reason why the IASI data give



**Fig. 6.** Vertical profiles of 36-h forecast RMSEs for (a) wind speed ( $\text{m s}^{-1}$ ), (b) temperature (K), and (c) specific humidity ( $\text{g kg}^{-1}$ ), against conventional observations for CTRL, 3DVAR\_AM, and HYBRID\_AM. The numbers of conventional observations are shown on the right of each panel.



**Fig. 7.** Mean absolute track errors as a function of forecast lead time for (a) Vicente from 0000 UTC 20 to 1800 UTC 21 July 2012, and (b) Saola from 0000 UTC 30 to 1800 UTC 31 July 2012 for experiments 3DVAR-AM, 3DVAR-AMIA, HYBRID-AM, and HYBRID-AMIA.

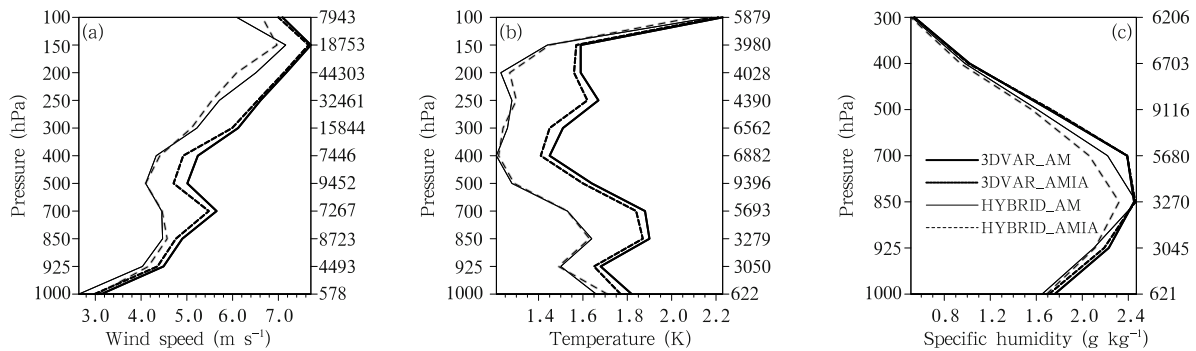


**Fig. 8.** As in Fig. 6, but for experiments 3DVAR-AM, 3DVAR-AMIA, HYBRID-AM, and HYBRID-AMIA.

better results in 3DVAR, but less promising results in the hybrid system is that, as an advanced data assimilation system, the hybrid system can make better use of limited observation information compared to 3DVAR. When more observations are assimilated in the hybrid system, the positive impacts are not significant, since the analyses from the hybrid system with only conventional and AMSU-A data are already satisfactory.

## 5. Summary and future perspectives

In this study, the WRFDA ETKF/3DVAR hybrid system is used to predict two typhoons using AMSU-A and IASI radiance data. The vertical localization

schemes are considered for radiance assimilation in the hybrid system. The results show that ETKF has some skill in updating the ensemble perturbations and maintaining the ensemble spread, corresponding to the forecast errors, especially for wind. The hybrid scheme provides a flow dependent background error with respect to the TC environment based on the ensemble performance. Model output is compared to TC “best tracks” and conventional observations. AMSU-A radiance data have slight positive impacts on the track forecast with the 3DVAR method. Typhoon track forecast skills are greatly improved when the hybrid scheme is employed. For 36-h forecasts, the hybrid scheme has lower RMSEs for wind, temperature at most levels, and specific humidity for at low levels,

compared to 3DVAR.

The assimilation of both AMSU-A and IASI radiance data in the ETKF/3DVAR hybrid system is also conducted. On average, the use of the IASI radiance data in the hybrid system upgrades the track, wind, and specific humidity forecast compared to the experiment without the IASI radiance in the hybrid system, but less significantly and consistently than the use of IASI radiances in 3DVAR compared to the experiment without IASI radiance in 3DVAR.

In this study, we use ETKF/3DVAR hybrid to investigate two typhoon cases. To assess the impact of radiance assimilation in the framework of ETKF/3DVAR hybrid on TCs, additional studies with more cases over extended periods are needed. As radiances are important in improving the quality of initial conditions of NWP systems, especially for TC forecasts, effective use of more radiance observations from other sensors should also be considered for future studies. Only track forecasts are emphasized in this study, since the intensity forecasts are not encouraging due to limitations of NWP in model dynamics, physical parameterizations, spatial resolution, etc. Further investigations into the use of the ETKF/3DVAR hybrid radiance data assimilation system for typhoon intensity forecasts are ongoing and will be reported in future papers.

As ETKF solves the Kalman filter equation in the ensemble space without localization, a single inflation factor is applied domain-wide. Sampling errors can easily cause instability issues (Bowler et al., 2008), especially for large non-physical perturbations. Further work is also planned to improve the inflation schemes in regional sub-domains or in a scale-dependent manner, to stabilize the ETKF scheme.

**Acknowledgments.** NCAR is sponsored by the US National Science Foundation. Any opinions, findings, and conclusions or recommendations expressed in this publication are those of the authors and do not necessarily reflect the views of the US National Science Foundation.

## REFERENCES

- Auligné, T., A. P. Dee, and D. P. McNally, 2007: Adaptive bias correction for satellite data in a numerical weather prediction system. *Quart. J. Roy. Meteor. Soc.*, **133**, 631–642.
- Barker, D. M., W. Huang, Y.-R. Guo, et al., 2004: A three-dimensional variational data assimilation system for MM5: Implementation and initial results. *Mon. Wea. Rev.*, **132**, 897–914.
- Barker, D. M., X.-Y. Huang, Z. Liu, et al., 2012: The Weather Research and Forecasting (WRF) model's community variational/ensemble data assimilation system: WRFDA. *Bull. Amer. Meteor. Soc.*, **93**, 831–843.
- Bishop, C. H., B. J. Etherton, and S. J. Majumdar, 2001: Adaptive sampling with the ensemble transform Kalman filter. Part I: Theoretical aspects. *Mon. Wea. Rev.*, **129**, 420–436.
- Blumstein, D., G. Chalon, T. Carlier, et al., 2004: IASI instrument: Technical overview and measured performances. *Proceedings of SPIE*, **5543**, 196–207.
- Bowler, N. E., A. Arribas, K. R. Mylne, et al., 2008: The MOGREPS short-range ensemble prediction system. *Quart. J. Roy. Meteor. Soc.*, **134**, 703–722.
- Cavallo, S. M., J. Dudhia, and C. Snyder, 2011: A multi-layer upper-boundary condition for longwave radiative flux to correct temperature biases in a mesoscale model. *Mon. Wea. Rev.*, **139**, 1952–1959.
- Chen, F., and J. Dudhia, 2001: Coupling an advanced land-surface/hydrology model with the Penn State/NCAR MM5 modeling system. Part I: Model description and implementation. *Mon. Wea. Rev.*, **129**, 569–585.
- Chou, M. D., and M. J. Suarez, 1994: An efficient thermal infrared radiation parameterization for use in general circulation models. NASA Tech. Memo., Maryland, 85 pp.
- Dee, D. P., and S. M. Uppala, 2009: Variational bias correction of satellite radiance data in the ERA-Interim reanalysis. *Quart. J. Roy. Meteor. Soc.*, **135**, 1830–1841.
- Derber, J. C., and W. S. Wu, 1998: The use of TOVS clear-sky radiances in the NCEP SSI analysis system. *Mon. Wea. Rev.*, **126**, 2287–2299.
- Dowell, D. C., F. Zhang, L. J. Wicker, et al., 2004: Wind and temperature retrievals in the 17 May 1981 Arcadia, Oklahoma, supercell: Ensemble Kalman filter experiments. *Mon. Wea. Rev.*, **132**, 1982–2005.
- Evensen, G., 1994: Sequential data assimilation with a nonlinear quasi-geostrophic model using Monte Carlo methods to forecast error statistics. *J. Geophys. Res.*, **99**, 10143–10162.

- Hamill, T. M., and C. Snyder, 2000: A hybrid ensemble Kalman filter—3D variational analysis scheme. *Mon. Wea. Rev.*, **128**, 2905–2919.
- Hamill, T. M., J. S. Whitaker, M. Fiorino, et al., 2011a: Global ensemble predictions of 2009’s tropical cyclones initialized with an ensemble Kalman filter. *Mon. Wea. Rev.*, **139**, 668–688.
- Hamill, T. M., J. S. Whitaker, D. T. Kleist, et al., 2011b: Predictions of 2010’s tropical cyclones using the GFS and ensemble-based data assimilation methods. *Mon. Wea. Rev.*, **139**, 3243–3247.
- Han, Y., P. Van Delst, Q. H. Liu, et al., 2006: JCSDA community radiative transfer model (CRTM)—Version 1. NOAA Tech. Rep. NESDIS, **122**, 33 pp.
- Hong, S.-Y., J. Dudhia, and S.-H. Chen, 2004: A revised approach to ice microphysical processes for the bulk parameterization of clouds and precipitation. *Mon. Wea. Rev.*, **132**, 103–120.
- Hong, S.-Y., Y. Noh, and J. Dudhia, 2006: A new vertical diffusion package with an explicit treatment of entrainment processes. *Mon. Wea. Rev.*, **134**, 2318–2341.
- Houtekamer, P. L., H. L. Mitchell, G. Pellerin, et al., 2005: Atmospheric data assimilation with an ensemble Kalman filter: Results with real observations. *Mon. Wea. Rev.*, **133**, 604–620.
- Kain, J. S., and J. M. Fritsch, 1990: A one-dimensional entraining/detraining plume model and its application in convective parameterization. *J. Atmos. Sci.*, **47**, 2784–2802.
- Li, Y. Z., X. G. Wang, and M. Xue, 2012: Assimilation of radar radial velocity data with the WRF hybrid ensemble-3DVAR system for the prediction of Hurricane Ike (2008). *Mon. Wea. Rev.*, **140**, 3507–3524.
- Liu, Q. H., and F. Z. Weng, 2006: Advanced doubling-adding method for radiative transfer in planetary atmosphere. *J. Atmos. Sci.*, **63**, 3459–3465.
- Liu, Z., C. S. Schwartz, C. Snyder, et al., 2012: Impact of assimilating AMSU-A radiances on forecasts of 2008 Atlantic tropical cyclones initialized with a limited-area ensemble Kalman filter. *Mon. Wea. Rev.*, **140**, 4017–4034.
- Lorenc, A. C., 1986: Analysis methods for numerical weather prediction. *Quart. J. Roy. Meteor. Soc.*, **112**, 1177–1194.
- Lorenc, A. C., 2003: The potential of the ensemble Kalman filter for NWP—A comparison with 4D-VAR. *Quart. J. Roy. Meteor. Soc.*, **129**, 3183–3203.
- McNally, A. P., and P. D. Watts, 2003: A cloud detection algorithm for high-spectral-resolution infrared sounders. *Quart. J. Roy. Meteor. Soc.*, **129**, 3411–3423.
- McNally, A. P., P. D. Watts, J. A. Smith, et al., 2007: The assimilation of AIRS radiance data at ECMWF. *Quart. J. Roy. Meteor. Soc.*, **132**, 935–957.
- Meng, Z., and F. Zhang, 2008: Tests of an ensemble Kalman filter for mesoscale and regional-scale data assimilation. Part IV: Comparison with 3DVAR in a month-long experiment. *Mon. Wea. Rev.*, **136**, 3671–3682.
- Mlawer, E. J., S. J. Taubman, P. D. Brown, et al., 1997: Radiative transfer for inhomogeneous atmosphere: RRTM, a validated correlated-k model for the long-wave. *J. Geophys. Res.*, **102**, 16663–16682.
- Parrish, D. F., and J. C. Derber, 1992: The National Meteorological Center’s spectral statistical interpolation analysis system. *Mon. Wea. Rev.*, **120**, 1747–1763.
- Schwartz, C. S., Z. Liu, Y. Chen, et al., 2012: Impact of assimilating microwave radiances with a limited-area ensemble data assimilation system on forecasts of Typhoon Morakot. *Wea. Forecasting*, **27**, 424–437.
- Schwartz, C. S., Z. Liu, X.-Y. Huang, et al., 2013: Comparing limited-area 3DVAR and hybrid variational-ensemble data assimilation methods for typhoon track forecasts: Sensitivity to outer loops and vortex relocation. *Mon. Wea. Rev.*, **141**, 4350–4372.
- Skamarock, W. C., J. B. Klemp, J. Dudhia, et al., 2008: A description of the advanced research WRF version 3. NCAR Tech. Note, NCAR/TN-4751STR, 113 pp.
- Torn, R. D., G. J. Hakim, and C. Snyder, 2006: Boundary conditions for limited-area ensemble Kalman filters. *Mon. Wea. Rev.*, **134**, 2490–2502.
- Torn, R. D., and G. J. Hakim, 2009: Ensemble data assimilation applied to RAINEX observations of Hurricane Katrina (2005). *Mon. Wea. Rev.*, **137**, 2817–2829.
- Wang, H., M. Mu, and X.-Y. Huang, 2011: Application of conditional nonlinear optimal perturbation to tropical cyclone adaptive observation using the Weather Research Forecasting (WRF) model. *Tellus A*, **63**, 939–957.
- Wang, H. L., and X.-Y. Huang, 2012: TAMDAR observation assimilation in WRF 3D-Var and its impact on Hurricane Ike (2008) Forecast. *Atmos. Oceanic Sci. Lett.*, **5**, 206–211.

- Wang, H. L., X.-Y. Huang, J. Sun, et al., 2014: Inhomogeneous background error modeling for WRF-Var using the NMC method. *J. Appl. Meteor. climatol.*, **53**, 2287–2309.
- Wang, X. G., 2011: Application of the WRF hybrid ETKF-3DVAR data assimilation system for hurricane track forecasts. *Wea. Forecasting*, **26**, 868–884.
- Wang, X. G., T. M. Hamill, J. S. Whitaker, et al., 2007: A comparison of hybrid ensemble transform Kalman filter-OI and ensemble square-root filter analysis schemes. *Mon. Wea. Rev.*, **135**, 1055–1076.
- Wang, X. G., D. M. Barker, C. Snyder, et al., 2008: A hybrid ETKF-3DVAR data assimilation scheme for the WRF model. Part II: Real observation experiments. *Mon. Wea. Rev.*, **136**, 5132–5147.
- Whitaker, J. S., T. M. Hamill, X. Wei, et al., 2008: Ensemble data assimilation with the NCEP Global Forecast System. *Mon. Wea. Rev.*, **136**, 463–482.
- Xu, D., Z. Liu, X.-Y. Huang, et al., 2013a: Impact of assimilating IASI radiance observations on forecasts of two tropical cyclones. *Meteor. Atmos. Phys.*, **122**, 1–18.
- Xu, D., A. P. Mizzi, and X.-Y. Huang, 2013b: Impact of TAMDAR data on Hurricane Paula with an eigen-structure dependent inflation scheme in the WRFDA/ETKF hybrid data assimilation system. 93rd American Meteorological Society Annual Meeting, Austin, Texas, USA, 1–6 January.
- Zhang, F., Y. Weng, J. A. Sippel, et al., 2009: Cloud-resolving hurricane initialization and prediction through assimilation of Doppler radar observations with an ensemble Kalman filter. *Mon. Wea. Rev.*, **137**, 2105–2125.